ACS Photonics

pubs.acs.org/journal/apchd5

Article

Modifying the Quality Factors of the Bound States in the Continuum in a Dielectric Metasurface by Mode Coupling

Zhaotang Li, Lidan Zhou, Zhuojun Liu,* Mingcheng Panmai, Shulei Li, Jin Liu, and Sheng Lan*

Cite This: *ACS Photonics* 2023, 10, 206−216

Read Online

ACCESS | Metrics & More | Article Recommendations | Supporting Information

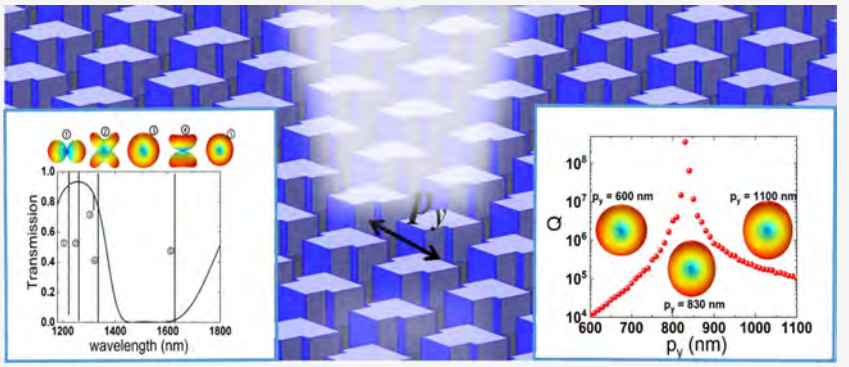

ABSTRACT: As optical resonances with high-quality (Q) factors, bound states in the continuum (BICs) supported in a metamaterial with low optical loss have attracted great interest due to their potential applications in photonic devices with different functionalities. However, most studies focus on the influence of the symmetry breaking in the constituent elements on the Q factors of the quasi-BICs, and less attention is paid to the coupling between the constituent elements. Here, we investigate numerically and experimentally the quasi-BICs revealed in metasurfaces composed of regularly arranged silicon (Si) nanoparticles with and without a geometric symmetry. It is found that the quasi-BICs appear in the transmission spectra of the metasurfaces as Fano lineshapes with different asymmetry parameters, depending strongly on the relative locations of the two optical modes involved in the interference. Apart from symmetry-protected BICs dominated by optical modes that radiate only in the direction parallel to the metasurface, accidental BICs at-Γ formed by the destructive interference of two optical modes are also revealed. The leakage of the quasi-BICs in the direction of light incidence originates from the interference of such modes with other optical modes existing in the same spectral range, which limits the maximum Q factors of the quasi-BICs. Consequently, quasi-BICs with high-Q factors (10^{10} to 10^{13}) are also observed in metasurfaces composed of Si nanoparticles with geometric symmetry (or without symmetry breaking). More interestingly, the Q factors of the quasi-BICs in a metasurface composed of Si nanoparticles with symmetry breaking exhibit a strong dependence on the period of the metasurface. An exponential decrease of the Q factor is observed when the period of the metasurface deviates from the value at which the maximum Q factor is achieved, implying the crucial role of mode coupling in determining the Q factor. As a result, the Q factor of a quasi-BIC may not decrease exponentially when the symmetry breaking of the Si nanoparticle is increased. In comparison, the quasi-BICs in a metasurface composed of Si nanoparticles with geometric symmetry are not sensitive to the period of the metasurface. By deliberately choosing the period, the maximum Q factors of the quasi-BICs achieved in the metasurface with symmetry breaking are close to those realized in the metasurface without symmetry breaking. Our findings are important for understanding the physical origin of the so-called symmetry-protected BICs supported by metasurfaces and helpful for designing photonic devices based on quasi-BICs.

KEYWORDS: *metasurface, bound state in the continuum, silicon nanoparticle, Mie resonance, mode coupling*

INTRODUCTION

Optical resonances represent specific wavelengths at which the interaction between optical materials and light is greatly enhanced.[1,2] They are usually manifested as peaks or dips in the transmission/reflection spectrum of an optical material. In the past decade, metamaterials and metasurfaces composed of artificial atoms have attracted great interest because of their abilities in controlling the amplitude, phase, and polarization of light.[3−8] In the visible to near-infrared spectral range, metallic

Received: September 19, 2022
Published: December 23, 2022

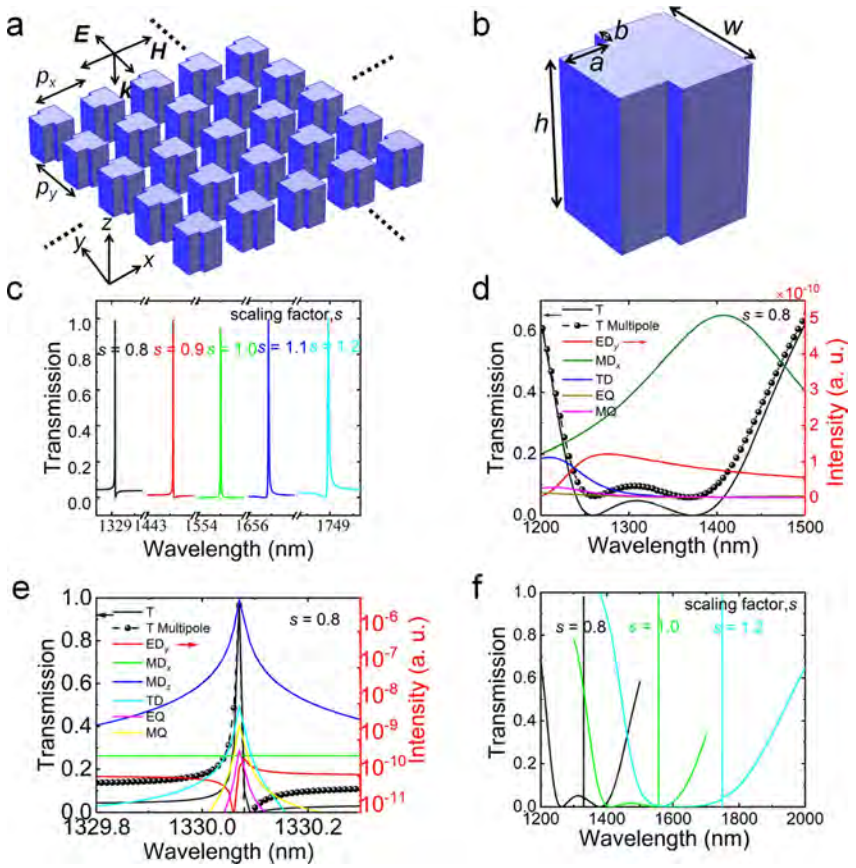

Figure 1. (a) Schematic showing a dielectric metasurface composed of periodically arranged Si cuboids with symmetry breaking in the *xy* plane. The periods in the *x* and *y* directions are p_x and p_y. The plane wave is incident along the −*z* direction, with electric and magnetic fields oscillating in the *y* and *x* directions. (b) Geometrical structure of a single Si cuboid. (c) Transmission spectra calculated for the metasurfaces with different scaling parameters *s*. (d) Transmission spectrum of the metasurface with *s* = 0.8 and its decomposition into Mie resonances in the wavelength range of 1200−1500 nm. The transmission spectrum reconstructed by using the multipole decomposition method is also provided for comparison. (e) Transmission spectrum of the quasi-BIC revealed in the metasurface with *s* = 0.8 and its decomposition into Mie resonances in the wavelength range of 1329.8−1330.3 nm. The transmission spectrum reconstructed by using the multipole decomposition method is also provided for comparison. (f) Transmission spectra calculated for the metasurfaces with scaling parameters of *s* = 0.8, 1.0, and 1.2.

nanoparticles with different shapes are usually used to construct metamaterials/metasurfaces because they support surface plasmon resonances. Owing to the Ohmic loss of metals, however, optical resonances with high-quality (*Q*) factors are not expected for such metamaterials/metasurfaces.[9−12] In recent years, metamaterials/metasurfaces constructed with high-index dielectric nanoparticles, such as silicon (Si) nanoparticles, have become the focus of many studies because such nanoparticles support Mie resonances in which enhanced field localization and reduced Ohmic loss can be simultaneously achieved.[13] As compared with their metallic counterparts, the most important advantage of dielectric metamaterials is the achievement of optical resonances with ultrahigh-*Q* factors.[14] Therefore, strong light-matter interaction, which is crucial for nonlinear optics and quantum electrodynamics, can be realized by exploiting these high-*Q* optical resonances formed in dielectric metamaterials.

Very recently, bound states in the continuum (BICs) have received intensive studies because of their high-*Q* factors, which imply potential applications in lasers,[15,16] harmonic generation,[17−19] sensing[20−22] and so forth. Physically, BICs with infinitely large *Q* factors exist only in metamaterials with infinite sizes at least in one dimension,[23−25] such as a two-dimensional metamaterial with infinite number of periods. They are clarified into two types, which are referred to as symmetry-protected BICs[24−28] and accidental (or Friedrich−Wintgen) BICs.[23,29−36] The former BICs are decoupled with the radiation continuum by the geometric symmetry of the constituent elements (or dielectric nanoparticles) with respect to the incident light by exploiting mainly the dark axis of an electric dipole (ED) or a magnetic dipole (MD). Breaking of symmetry can be realized by using an oblique incidence or by introducing defects in dielectric nanoparticles.[24,37−45] As a result, quasi-BICs with reduced *Q* factors can be readily revealed in transmission/reflection spectrum of a metasurface. It is generally accepted that symmetry-protected BICs cannot be excited unless the symmetry is broken.[40,44,46] In addition, it is found that the *Q* factor of a quasi-BIC decreases exponentially with increasing asymmetry.[37] However, a dielectric nanoparticle with a finite size may simultaneously support multiple modes which are not isolated from each other. The interaction between them may modify more or less their radiation properties, leading to the leakage of the optical modes, which are expected to be decoupled with radiation continuum.[47] In a recent study,[48] directional lasing was successfully demonstrated by exploiting the symmetry-protected BIC formed in a regular array of GaAs nanocylinders. It was revealed that the emission spectrum of the

https://doi.org/10.1021/acsphotonics.2c01461
ACS Photonics 2023, 10, 206−216

array can be modified by changing the period of the array, governing the coupling between GaAs nanocylinders. However, the influences of the coupling between dielectric nanoparticles on the Q factor of the quasi-BIC, especially in the metasurfaces composed of dielectric nanoparticles with defects, remain unexplored. Previously, it was found that propagating modes can be excited in a one-dimensional chain of dielectric nanoparticles via the activation of the MD of a dielectric nanoparticle in the chain.[49] It implies that the coupling between the constituent elements plays a crucial role in determining the radiation loss of the propagating modes in a one- and two-dimensional metamaterial. Therefore, it becomes quite important to understand the physical origin of the quasi-BICs excited in dielectric metasurfaces in order to design photonic devices for practical applications.

In this article, we investigated the quasi-BICs formed in metasurfaces composed of Si-based elements with and without symmetry breaking, including Si cuboids, cylinders, and spheres. We focused mainly on the quasi-BICs revealed in the transmission spectra of the metasurfaces, including symmetry-protected BICs and accidental BICs at-Γ. We examined the influences of the coupling between dielectric nanoparticles on the Q factors of these quasi-BICs by varying the periods of the metasurfaces. We found that high-Q quasi-BICs are formed not only in metasurfaces without symmetry breaking but also in those with symmetry breaking. We showed that the mode coupling between the constituent elements, which is governed by the periods of a metasurface, plays a crucial role in determining the Q factors of quasi-BICs in metasurfaces with symmetry breaking. We revealed that the physical origin limiting the Q factors of the quasi-BICs in a metasurface is mode interference.

RESULTS AND DISCUSSION

In this work, we investigated numerically and experimentally the quasi-BICs supported by metasurfaces composed of Si nanoparticles with and without symmetry breaking. In the numerical simulations, we considered infinite metasurfaces placed on the *xy* plane and suspended in air. In each case, the plane wave is normally incident on the metasurface along the $-z$ direction, with electric and magnetic fields oscillating in the *y* and *x* directions. We first examined a metasurface composed of periodically arranged Si cuboids with defects (i.e., a symmetry breaking is introduced with respect to the *yz* plane), as schematically shown in Figure 1a. The periods of the metasurface in the *x* and *y* directions are denoted as p_x and p_y. The geometry of the Si cuboid is characterized by the structural parameters *w*, *h*, *a*, and *b*, as shown in Figure 1b. Here, *w* represents the length and width of the Si cuboid, while *h* represents its height. The length and width of the defect are denoted by *a* and *b*. Based on a previous study,[45] such a metasurface supports a quasi-BIC governed by an MD oriented in the *z* direction (MD_z). In the middle of Figure 1c, we show the transmission spectrum (green curve) calculated for a metasurface with $p_x = p_y = 720$ nm, $w = 400$ nm, $h = 500$ nm, $a = 160$ nm, and $b = 60$ nm. In this case, it is noticed that the quasi-BICs exhibit a symmetric Lorentz lineshape. By introducing a scaling factor *s*, we can change the size of the Si cuboid while keeping its geometry. In Figure 1c, we also present the transmission spectra calculated for metasurfaces composed of Si cuboids with reduced and enlarged sizes. The periods of the metasurfaces remain unchanged, while the geometry of the Si cuboid is characterized by $h = 500$ nm, $w = 400 \times s$ nm, $a = 160 \times s$ nm, and $b = 60 \times s$ nm, with $s = 0.8$, 0.9, 1.0, 1.1, and 1.2. It can be seen that the resonant wavelength of the quasi-BIC can be easily tuned in a wide spectral range by simply varying *s*. When *s* is changed from 0.8 to 1.2, the resonant wavelength of the quasi-BIC is shifted from ∼1100 to ∼1750 nm. In addition, it is noticed that the quasi-BICs of the five metasurfaces appear as Fano lineshapes characterized by asymmetry parameters *q* with different values ranging from negative to positive value. The symmetric Lorentz lineshape observed at $s = 1.0$ can be considered as a Fano lineshape with $q = \infty$. It is well known that a Fano resonance is generated through the interference of a broad mode (superradiant mode) and a narrow mode (subradiant mode). The lineshape of the Fano resonance is determined by the phase difference between the two modes. This phenomenon indicates clearly that the quasi-BIC supported by a metasurface originates from the interference of at least two optical modes.

In order to find out the two modes involved in the interference, we performed multipolar expansion analysis (see the Supporting Information, Note 1) for the quasi-BIC formed with $s = 0.8$, as shown in Figure 1d,e. In Figure 1d, we show the transmission spectrum of the metasurface and the corresponding multipolar expansion in the wavelength range of 1200−1500 nm. In this case, the wavelength interval was intentionally chosen to be 5.0 nm, which is much wider than the linewidth of the quasi-BIC, in order to see the broad modes. One can see two transmission dips located at ∼1260 and ∼1380 nm, which are dominated by ED oriented in the *y* direction (i.e., ED_y) and MD oriented in the *x* direction (i.e., MD_x), respectively. In Figure 1e, we present the transmission spectrum of the metasurface and the corresponding multipolar expansion in a narrow wavelength range of 1329.8−1330.3 nm, which is obtained by using a small wavelength interval of 0.01 nm. In general, the multipole decomposition method is used to analyze the Mie resonances that contribute to the scattering of a single dielectric nanoparticle. In this case, a perfectly matched layer boundary condition is employed. For a metasurface composed of a periodically arranged dielectric nanoparticles, the interaction between the constituent nanoparticles can be taken into account by using a periodic boundary condition. In this way, one can reveal the Mie resonances involved in the interference and the physical origins for the formation of quasi-BICs based on multipolar expansion analysis. In addition, the transmission and reflection spectra of the metasurface can be reconstructed.[46] Here, one can see an asymmetric Fano lineshape located at ∼1330 nm, which is governed by MD in the *z* direction (i.e., MD_z). In this case, the intensities of the broad modes (ED_y and MD_x) are 3 orders of magnitude weaker than that of the narrow mode (MD_z). Thus, they can only be revealed in a logarithmic coordinate. Therefore, it is revealed that the quasi-BIC with an asymmetric Fano lineshape is generated by the interference of MD_z with ED_y and MD_x. In order to verify the validity of the multipolar expansion analysis, we also reconstructed the transmission spectrum of the quasi-BIC with a modified multipole decomposition method.[46] As shown in Figure 1e, the reconstructed transmission spectrum is qualitatively in agreement with that obtained in the numerical simulation. In order to see the influence of the scaling factor *s* on the lineshape of the quasi-BIC, we show the transmission spectra of the metasurfaces with different values of *s* in a moderate wavelength range in Figure 1f. The wavelength interval around the quasi-BIC was intentionally chosen to be

https://doi.org/10.1021/acsphotonics.2c01461
ACS Photonics 2023, 10, 206−216

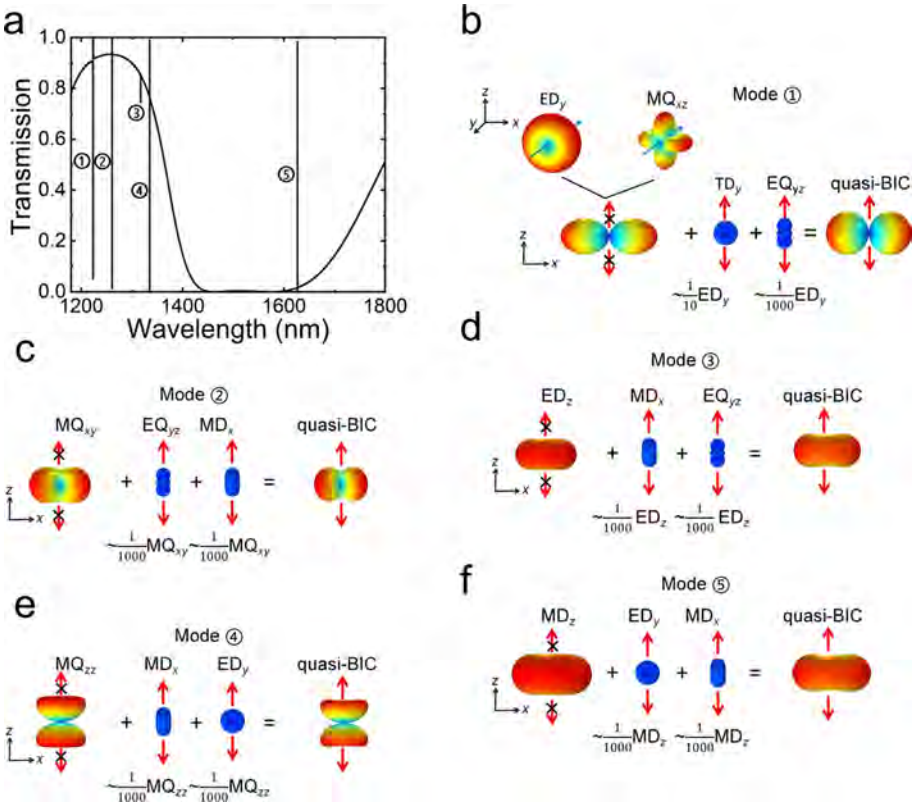

Figure 2. (a) Transmission spectrum calculated for the metasurface with structure parameters of p_x = 720 nm, p_y = 700 nm, w = 400 nm, h = 500 nm, a = 160 nm, and b = 20 nm in the wavelength range of 1180−1800 nm. The five high-Q resonances revealed in the transmission spectrum are marked by ①, ②, ③, ④, and ⑤. The physical origins of the five quasi-BICs (mode ①−mode ⑤) illustrated by the 3D radiation patterns of the Mie resonances involved in the interference are presented in (b−f).

narrow (0.01 nm). For s = 0.8, the wavelength of the narrow mode is smaller than that of the broad one (i.e., the narrow mode is located on the left side of the broad one). In this case, the q value of the Fano lineshape is negative. When s is increased to 1.0, the wavelength of the narrow mode coincides with that of the broad one because its wavelength shift with increasing s is larger than that of the broad mode. In this case, a symmetric Lorentz lineshape with $q = \infty$ is achieved. A further increase of s to 1.2 leads to an asymmetric Fano lineshape again with a positive q value because the narrow mode is moved to the right side of the broad one. We examined the dependence of the Q factor of the quasi-BIC on the scale factor s. It was found that the largest Q factor is not achieved in the symmetric Lorentz lineshape (see the Supporting Information, Note 2).

Now, we examine the high-Q optical resonances in a wide spectral range (1200−1800 nm) supported by a metasurface with p_x = 720 nm, p_y = 700 nm, w = 400 nm, h = 500 nm, a = 160 nm, and b = 20 nm, as shown in Figure 2a. One can identify five optical modes with high-Q factors (i.e., quasi-BICs), which are denoted as ①, ②, ③, ④, and ⑤. Apart from the quasi-BIC located at ∼1600 nm, there are other four quasi-BICs located in the short wavelengths (modes ①−④). Different from the quasi-BIC at ∼1600 nm, which appears as a Fano peak, the other four quasi-BICs appear as Fano dips in the transmission spectrum. In order to understand the physical origins of the five quasi-BICs revealed in the transmission spectrum of the metasurface, we performed multipolar expansion analyses for the scattering spectra of the Si cuboid and examined the electric and magnetic field distributions in the Si cuboid (see the Supporting Information, Note 3). We also confirmed that the transmission spectra of the quais-BICs can be reconstructed based on the multipole decomposition method (see the Supporting Information, Note 4). In Figure 2b−f, we present the three-dimensional (3D) radiation patterns of the Mie resonances involved in the mode interference that leads to the formation of the five quasi-BICs (i.e., modes ①−⑤). The physical origins for the quasi-BICs can be easily understood from the far-field radiation behaviors modified by the interference of Mie resonances. Mode ① is formed by the interference between ED_y and MQ_{xz} (magnetic quadrupole in the xz plane), which leads to the directional radiation in the x direction (or the cancelation of radiation in the z direction). Mode ② is governed by MQ_{xy} (magnetic quadrupole in the xy plane), which is manifested clearly in the electric and magnetic field distributions. Its radiation appears as four lobes in the xy plane with negligible leakage in the z direction. Mode ③ is dominated by an ED oriented in the z direction (i.e., ED_z), giving rise to a donut-shaped radiation pattern. Interestingly, mode ④ is governed by MQ_{zz}, which is composed of two out-of-phase MDs oriented in the z direction (i.e., MD_z). A clockwise circular electric field distribution is observed in the upper part of the Si cuboid, while an anti-clockwise circular one is found in the lower part, resulting in a diabolo-like radiation pattern. Mode ⑤ has been widely studied in the literature.[43−45,50−52] It is dominated by MD_z, with a donut-shaped radiation pattern and a dark axis in the z direction. Based on the above analysis, it is revealed that the quasi-BICs are governed by optical modes radiated in the xy direction (e.g., modes ②−⑤) or created by the destructive

https://doi.org/10.1021/acsphotonics.2c01461
ACS Photonics 2023, 10, 206−216

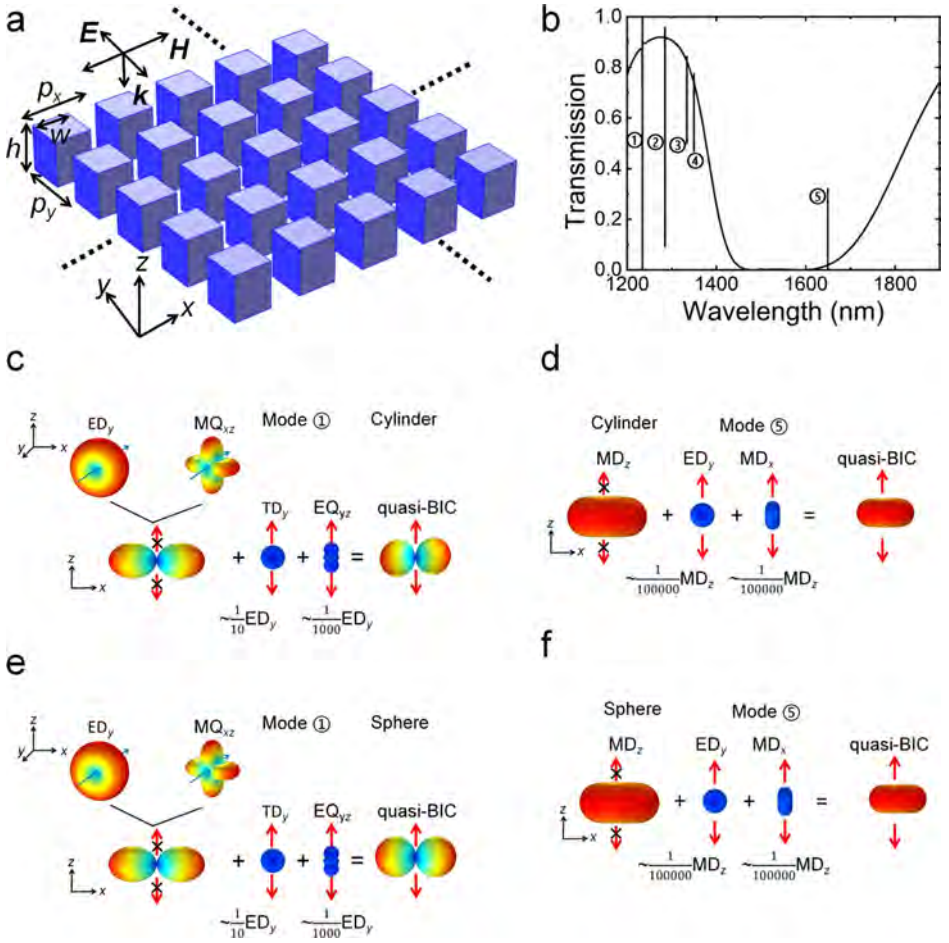

Figure 3. (a) Schematic showing a metasurface composed of periodically arranged Si cuboids without symmetry breaking in the *xy* plane. The periods in the *x* and *y* directions are p_x and p_y. The plane wave is incident along the −*z* direction with electric and magnetic fields oscillating in the *y* and *x* directions. (b) Transmission spectrum calculated for the metasurface with structure parameters of p_x = 720 nm, p_y = 700 nm, w = 400 nm, and h = 500 nm in the wavelength range of 1200−1900 nm. The five high-Q resonances revealed in the transmission spectrum are marked by ①, ②, ③, ④, and ⑤. (c) 3D radiation patterns of the Mie resonances involved in the interference showing the physical origin of mode ① formed in the metasurface composed of Si cylinders. (d) 3D radiation patterns of the Mie resonances involved in the interference showing the physical origin of mode ⑤ in the metasurface composed of Si cylinders. (e) 3D radiation patterns of the Mie resonances involved in the interference showing the physical origin of mode ① formed in the metasurface composed of Si spheres. (f) 3D radiation patterns of the Mie resonances involved in the interference showing the physical origin of mode ⑤ in the metasurface composed of Si spheres.

interference of two optical modes (e.g., mode ①). In the former case, the *z* axis is the dark axis of the dominated modes. In the latter case, the interference of two optical modes leads to the cancelation of the radiation in the *z* direction. In all cases, the quasi-BICs are formed by the interference of the dominant Mie resonances (subradiant) with the background Mie resonances (superradiant), leading to Fano lineshapes. Although the intensities of the latter are several orders of magnitudes weaker than those of the former, the interaction between them leads to the leakage of the dominant Mie resonances and limits the *Q* factors of the quasi-BICs. For example, the interference of MD_z with ED_y and MD_x, which are 3 orders of magnitude weaker than that of MD_z, leads to the leakage of MD_z in the *z* direction and limits the *Q* factor of this quasi-BIC (see Figure 2f). The wavelengths, *Q* factors, and enhancement factors for electric and magnetic fields are presented in Table S1 (see the Supporting Information, Note 5). In general, it was found that a quasi-BIC with a higher *Q* factor will possess larger enhancement factors for electric and magnetic fields (see the Supporting Information, Note 5).

So far, we have investigated the quasi-BICs formed in metasurfaces composed of Si cuboids with defects. These quasi-BICs usually have low *Q* factors, which can be readily revealed in the transmission spectra of the metasurfaces. Now we examine a metasurface composed of Si cuboids without defects, as schematically shown in Figure 3a. The structural parameters of the metasurface were chosen to be p_x = 720 nm, p_y = 700 nm, w = 400 nm, and h = 500 nm, which are exactly the same as those used for the metasurface with defect. In this way, we can easily compare the quasi-BICs formed in the two types of the metasurfaces. Surprisingly, the five quasi-BICs found in the metasurface with defect are still observed in the metasurface without defect, as manifested in the transmission spectrum shown in Figure 3b. The multipolar expansion analyses for these modes reveal the same physical origins as those observed in the metasurface with defect (not shown). The electric/magnetic field distributions calculated for these modes further confirm that they are the same optical modes observed in the metasurface with defect (see the Supporting Information, Note 6). We also examined the resonant wavelengths, *Q* factors, and enhancement factors for electric

https://doi.org/10.1021/acsphotonics.2c01461
ACS Photonics 2023, 10, 206−216

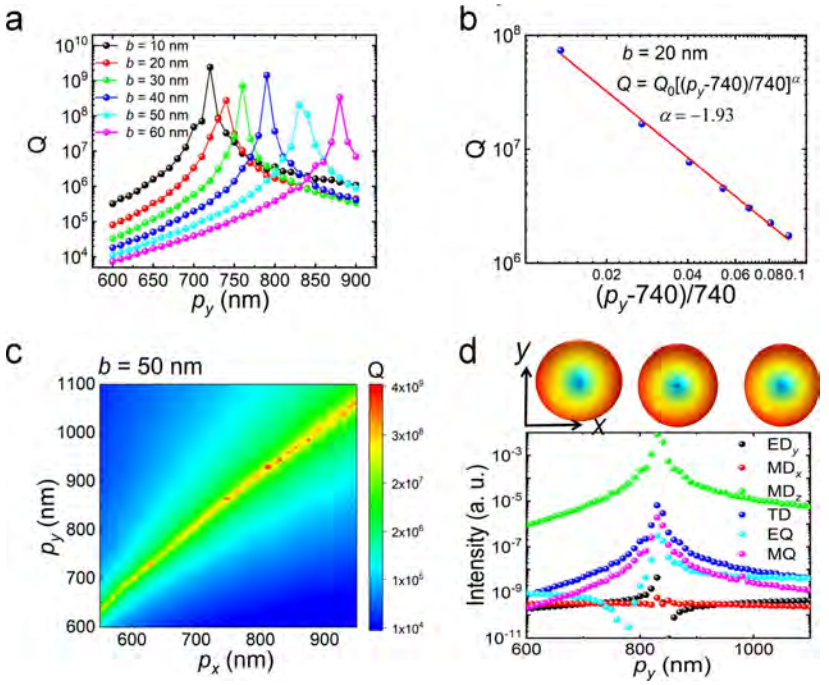

Figure 4. (a) Dependence of the *Q* factor of the quasi-BIC on the period in the *y* direction (p_y) obtained for metasurfaces with different symmetries (*b* values). (b) Dependence of the *Q* factor of the quasi-BIC on the deviation from the optimum period ($p_y - 740$)/740 for the metasurface with *b* = 20 nm plotted in a logarithmic coordinate. (c) Dependence of the *Q* factor of the quasi-BIC on the periods in the *x* and *y* directions (p_x and p_y) for the metasurface with *b* = 50 nm. (d) Multipolar decompositions of the quasi-BICs formed in the metasurface with *b* = 50 nm, p_x = 720 nm and different periods in the *y* direction (p_y). The radiation patterns in the *xy* planes calculated at different periods in the *y* direction (p_y = 600, 830, and 1100 nm) are shown as insets.

and magnetic fields for the five quasi-BICs (see the Supporting Information, Note 7). It was found that the resonant wavelength of each quasi-BIC is red-shifted with respect to that of the quasi-BIC observed in the metasurface with defect. This is because the elimination of the defect is equivalent to the increase in the volume of the Si cuboid. As expected, the quasi-BICs supported by the metasurface without defect possess higher *Q* factors and larger field enhancement factors as compared with those supported by the metasurface with defect. The introduction of defect breaks the geometric symmetry of the Si cuboid, leading to more leakage of energy into the *z* direction.

In order to confirm the existence of quasi-BICs in metasurfaces without defect (i.e., without symmetry breaking in the geometry of Si nanoparticle), we also studied the metasurfaces composed of Si cylinders and Si spheres, as schematically shown in Figure S4a,b (see the Supporting Information, Note 8). In Figure 3c,d, we show the 3D radiation patterns simulated for two quasi-BICs (modes ① and ⑤) revealed in the transmission spectra (see the Supporting Information, Note 9) of a metasurface composed of Si cylinders with a diameter of d = 440 nm and a height of h = 500 nm. The periods of the metasurface were set as $p_x = p_y$ = 720 nm. The electric/magnetic field distributions in the Si cylinder are also examined (see the Supporting Information, Note 9). It is revealed that mode ① arises from the interference of ED_y and MQ_{xz} and exhibits an 8-shaped radiation pattern. It has a *Q* factor of 3.0×10^5. In comparison, mode ⑤ governed by MD_z possesses a much higher *Q* factor of 2.09×10^8, which is limited by the interference with ED_y and MD_x. In Figure 3e,f, we present the 3D radiation pattern for the same two quasi-BICs revealed (modes ① and ⑤) in the transmission spectra (see the Supporting Information, Note 9) of a metasurface ($p_x = p_y$ = 720 nm) composed of Si spheres with a diameter of d = 500 nm. The physical origins for the formation of the quasi-BICs can be easily understood. Based on the multipolar expansion analyses, it is found that mode ① (Q = 183) is created by the interference of ED_y and MQ_{xz}, while mode ⑤ ($Q = 2.68 \times 10^8$) is dominated by MD_z.

Based on the results presented above, we can conclude that the quasi-BIC dominated by MD_z is commonly observed in metasurfaces composed of elements of different shapes (cuboid, cylinder, sphere, etc.) with or without defect. For metasurfaces composed of elements without defect, this quasi-BIC generally possesses a *Q* factor as high as $\sim 10^8$ (or a linewidth as small as 10^{-5} to 10^{-6} nm) together with an enhancement factor as large as 10^4 to 10^5. For this reason, this quasi-BIC is difficult to be resolved in the transmission spectra measurements of the metasurfaces. Even in numerical simulations, the wavelength interval should be set at the same level of the linewidth in order to reveal this quasi-BIC. Physically, the *Q* factor of this quasi-BICs is limited by the existence of other Mie resonances (e.g., the broad modes ED_y and MD_x) although their intensities are orders of magnitude weaker than that of MD_z. The leakage in the *z* direction originates from the interference of these Mie resonances with MD_z. Relying on numerical simulation, we confirmed that the quasi-BIC dominated by MD_z can be excited by an ED source oriented in the *y* direction (i.e., ED_y) or an MD source oriented in the *x* direction (i.e., MD_x), which are placed at the center of the Si cuboid (see the Supporting Information, Note 10). This behavior indicates that the existence of ED_y and MD_x and their interaction with MD_z provide a channel for coupling the incident wave into MD_z and the radiation of MD_z into the

https://doi.org/10.1021/acsphotonics.2c01461
ACS Photonics 2023, 10, 206−216

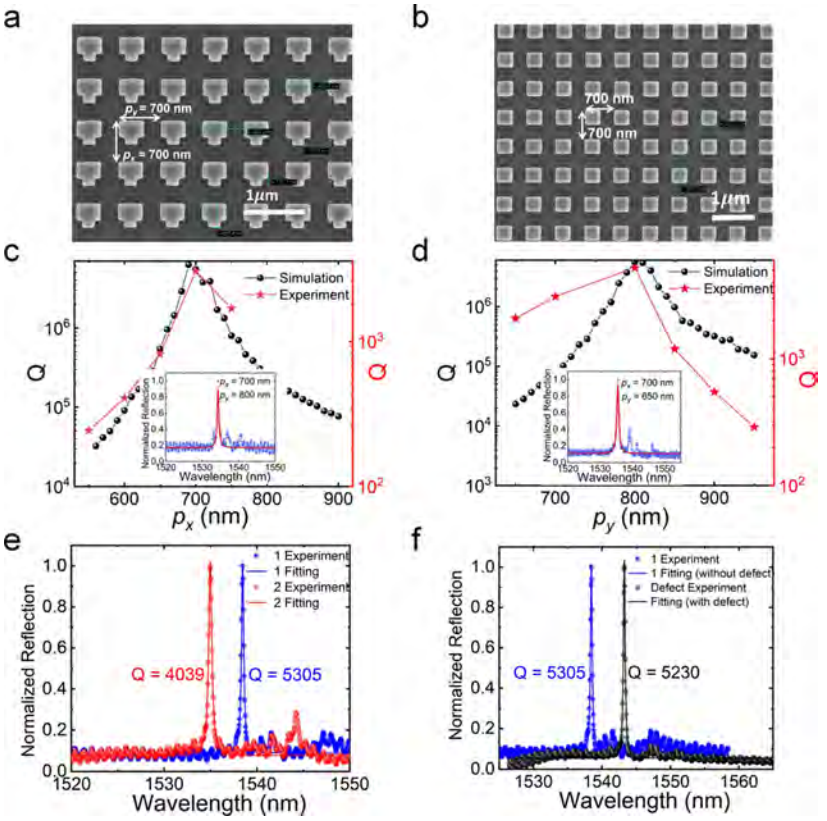

Figure 5. SEM images of the metasurfaces with (a) and without (b) defects. The dependences of the Q factor of the quasi-BIC on the periods in the x and y directions (p_x and p_y) calculated and measured for the metasurface with defects (a = 120 nm and b = 100 nm) are shown in (c) and (d), respectively. (e) Reflection spectra of the two metasurfaces without defects showing quasi-BICs; the fittings of the reflection spectra by using Lorentz lineshapes are also provided. (f) Reflection spectra of the metasurfaces without (w = 370 nm, h = 500 nm, and $p_x = p_y$ = 700 nm) and with (w = 400 nm, h = 500 nm, a = 120 nm, b = 100 nm, p_x = 700 nm, and p_y = 800 nm) defects; the fittings of the reflection spectra by using Lorentz lineshapes are also provided.

continuum. The introduction of a defect in the constituent element will distort to some extent the electric and magnetic field distributions in the element, which increases the energy loss and reduces the Q factor.

Apart from the introduction of defect, we reveal that the coupling between the constituent elements, which is governed by the period of a metasurface, also influences significantly the Q factors of the quasi-BICs in a metasurface with defect. This feature can be employed to manipulate the Q factors of quasi-BICs. In Figure 4a, we present the dependence of the Q factor of the quasi-BIC on the period (p_y) calculated for metasurfaces composed of Si cuboids with different defects (characterized by parameter b). Here, p_x was fixed at 720 nm. Interestingly, a rapid increase of the Q factor is observed with increasing p_y in each case. After reaching a maximum, the Q factor decreases quickly with increasing p_y. The value of p_y at which the maximum Q factor is achieved becomes larger with increasing b. For p_y < 720 nm, one can see a decrease of the Q factor with increasing b (i.e., increasing asymmetry). For p_y > 840 nm, the Q factor may have larger value when b is increased. In each case (for the same b), a red shift of the quasi-BIC was observed with increasing p_y (see the Supporting Information, Note 11). A similar phenomenon was also observed when we fixed p_y and changed p_x (see the Supporting Information, Note 11). As an example, we examined the dependence of the Q factor of the quasi-BIC on the parameter b for a metasurface with p_x = 720 nm and p_y = 840 nm (see the Supporting Information, Note 12). It was found that the Q factor decreases initially with increasing b, reaching a minimum value of ~10^6 at b ~ 30 nm. After that, the Q factor increases exponentially to the maximum value of ~10^8 at b = 50 nm with increasing b and decreases exponentially with a further increase of b. This is a counterintuitive behavior, which implies the important role of the mode coupling in determining the Q factor of a quasi-BIC.

For the metasurface with b = 20 nm, the maximum Q factor is observed at p_y = 740 nm. In this case, the increased radiation induced by the defect is compensated by mode coupling, and a Q factor close to that observed in the metasurface without defect is achieved. Therefore, the deviation of the period of a metasurface from the optimum value, which is defined as $(p_y - 740)/740$, can be considered as an asymmetry introduced in the metasurface. Based on previous studies,[37] a slope of ~−2.0 is expected if the dependence of the Q factor on the asymmetry parameter is plotted in a logarithmic coordinate. In Figure 4b, we plot the dependence of the Q factor on the deviation from the optimum period [i.e., $(p_y - 740)/740$] in a logarithmic coordinate. As expected, a linear relationship is observed, implying that the Q factor of the quasi-BIC decreases exponentially with increasing period (p_y) from the optimum period. The slope extracted from the linear fitting in the range of $0 < (p_y - 740)/740 < 0.10$ was found to be ~−1.93, which is in good agreement with the value (−2.0) predicted from theoretical analysis.[37]

In Figure 4c, we present the Q factor of the quasi-BIC as functions of the periods in both the x and y directions (p_x and p_y). It can be seen that for each p_y, there exists a corresponding

https://doi.org/10.1021/acsphotonics.2c01461
ACS Photonics 2023, 10, 206−216

p_x at which the maximum Q factor is achieved and vice versa. Interestingly, it is remarkable that the paired periods (p_x, p_y) for the maximum Q factor are located on a straight line. In addition, it is found that the Q factors of the quasi-BICs are larger when p_x is chosen to be 750−870 nm compared to when p_y is chosen to be 850−970 nm. This behavior implies that appropriate periods in both directions are important for achieving large Q factors. For small periods, the energy is concentrated at the gap region between neighboring cuboids, leading to the leakage of the energy. For large periods, the coupling between neighboring cuboids becomes weak, and each cuboid behaves as an isolated one. In this case, a larger energy loss is also expected.

In order to gain a deep insight into the influence of the period on the Q factor of a quasi-BIC, we examined a metasurface with b = 50 nm and p_x = 720 nm. The other parameters remained unchanged. In Figure 4d, we present a multipolar expansion analysis for the Mie resonances involved in the interference at different periods (p_y). In this case, the maximum Q factor is observed at p_y = 830 nm. It can be seen that MD_z increases exponentially when p_y approaches 830 nm. In contrast, the other two modes (ED_y and MD_x) participating in the interference are not sensitive to the variation of the period. As a result, the leakage induced by the involvement of ED_y and MD_x becomes more significant when the period deviates from 830 nm. To further confirm this suspect, we calculated the radiation patterns at three different values of p_y = 600, 830, and 1100 nm, as shown in the insets. It is noticed that the top view of the radiation pattern at p_y = 600 nm appears as an ellipse with its long axis in the x direction. For p_y = 830 nm, the radiation pattern becomes a circle. It implies that the radiation is completely dominated by MD_z and the influences of ED_y and MD_x are negligible. As p_y is further increased to p_y = 1100 nm, an elliptical radiation pattern is observed again, with its long axis in the y direction. Similar phenomena are observed for metasurfaces with different structural parameters (see the Supporting Information, Note 13). The enhancements of electric and magnetic fields are important for enhancing light-matter interaction for various practical applications. As expected, the enhancement factors for electric and magnetic fields increase with increasing Q factors of quasi-BICs (see the Supporting Information, Note 14).

As discussed above, the Q factors of quasi-BICs supported by a metasurface with defect exhibit a strong dependence on the periods of the metasurface. We also examined the quasi-BICs in metasurfaces without defect. It is found that the Q factors of the quasi-BICs supported in such a metasurface are not sensitive to the periods of the metasurface (see the Supporting Information, Note 15). A small fluctuation in the Q factor, which exhibits a value in the range of 10^{10} to 10^{13}, is observed when the period is changed.

In order to verify the simulation results presented above, we fabricated metasurfaces composed of Si cuboids with and without defect by using the combination of electron beam lithography and reactive ion etching (see Methods for the details). In previous studies,[45] the metasurfaces were usually fabricated on a SiO_2 substrate by using wafer bonding technique. In this work, the metasurfaces used in the optical characterization were fabricated directly by using an SOI wafer (see Methods). It means that the metasurfaces were supported by a SiO_2/Si substrate, in which the thicknesses of the SiO_2 and Si were ∼2.0 and ∼725 μm. In this case, the transmission spectra could not be measured because of the weak transmitted signals. For this reason, we employed the reflection spectra measurements to reveal the quasi-BICs of the metasurfaces, which have been used in previous studies.[53] In each case, the metasurface is composed of 100 × 100 elements. In Figure 5a,b, we show the scanning electron microscopy (SEM) images of the metasurfaces with (w = 400 nm, h = 500 nm, a = 120 nm, b = 100 nm, and p_x = p_y = 700 nm) and without (w = 370 nm, h = 500 nm, and p_x = p_y = 700 nm) defect. In Figure 5c, we present the dependence of the Q factor of the quasi-BIC calculated and measured for the metasurface with defect on the period in the x direction (p_x). The period in the y direction was fixed at p_y = 800 nm. The Q factors of the quasi-BICs were derived from the reflection spectra measured for the metasurfaces by using cross-polarization white light source. This method has been used in the characterization of the quasi-BICs supported by metasurfaces.[53] It is noticed that the measured Q factors are 3 orders of magnitude smaller than the simulated ones. There are several reasons that are responsible for the discrepancies. First, we employed a periodic boundary in the numerical simulations, which implies infinite sizes for the metasurfaces. Therefore, the finite size of the fabricated samples (100 × 100 elements) will lead to a reduction in the Q factor of the quasi-BIC. Second, the thickness of the Si substrate was set as 2.0 μm in the numerical simulations, which is limited by the computation resources. However, the actual thickness of the Si substrate is 725 μm. Although the absorption of the Si at ∼1500 nm is quite small, the thick Si substrate also results in a dramatic reduction in the Q factor. Finally, the disorders and imperfections inevitably induced in the fabrication process also cause smaller Q factors, especially in the case of a high-Q factor. Despite the discrepancies in the absolute values of the Q factors, the measured Q factor exhibits a dependence on p_x similar to that of the simulated one, as shown in Figure 5c. When p_x is increased from 550 to 700 nm, the measured Q factor is increased from ∼244 to ∼3070, while the simulated one is increased from 3.3×10^4 to 6.0×10^6. The reflection spectrum measured for the metasurface with p_x = 700 nm is shown in the inset. The linewidth of the quasi-BIC, which is located at ∼1535 nm, is extracted to be ∼0.50 nm based on the fitting with a Lorentz lineshape. Thus, the Q factor in this case is derived to be ∼3070. This behavior indicates clearly the effect of the period on the Q factor of the quasi-BIC. When p_x is further increased to 750 nm, the Q factor is reduced to ∼1698. For metasurfaces with p_x >750 nm (p_x = 800, 850, and 900 nm), the quasi-BICs of the metasurfaces are beyond the detection limit of the InGaAs photodetector (<1600 nm) because the resonant wavelength of the quasi-BIC is shifted to longer wavelengths with increasing period. We also examined the dependence of the Q factor on the period in the y direction (p_y) when the period in the x direction is fixed (p_x = 700 nm). The simulated and measured results are compared in Figure 5d. Ignoring the absolute values of the Q factors, similar dependences of the Q factor on the period in the y direction (p_y) are observed in the simulated and measured results. When p_y is increased from 650 to 950 nm, the simulated Q factor increases exponentially from 2.3×10^4 to 5.6×10^6 and then decreases exponentially to 1.5×10^5. Similarly, the measured Q factor increases from ∼2086 to ∼5023 and then decreases to ∼290. In the inset of Figure 5d, we show the reflection spectrum obtained for a metasurface with p_y = 650 nm. The Q factor of the quasi-BIC extracted by using Lorentz fitting is found to be ∼2086.

https://doi.org/10.1021/acsphotonics.2c01461
ACS Photonics 2023, 10, 206−216

Except the metasurfaces with defect, we also examined the metasurfaces without defect. In Figure 5e, we show the reflection spectra measured for two metasurfaces without defect. They have exactly the same designed structural parameters (w = 370 nm, h = 500 nm, and $p_x = p_y$ = 700 nm). Due to the fabrication imperfections, it can be seen that the resonant wavelengths of the two quasi-BICs are different by ∼3.0 nm. However, the Q factors of the quasi-BICs extracted from the Lorentz fitting are quite similar (∼5305 and ∼4039). In Figure 5f, we compared the reflection spectra of two metasurfaces with and without defects. The structural parameters of the metasurface with defect are optimized to achieve a maximum Q factor (w = 400 nm, h = 500 nm, a = 120 nm, b = 100 nm, p_x = 700 nm, and p_y = 800 nm). In this case, the Q factor of the quasi-BIC supported by the metasurface with defect (∼5230) can be close to that of the quasi-BIC supported by the metasurface without defect (∼5305). It indicates undoubtedly that the Q factors of the quasi-BICs supported by a metasurface with defect can be modified by engineering the mode coupling between the constituent elements.

CONCLUSIONS

In summary, we have investigated the quasi-BICs formed in metasurfaces composed of elements with different geometries with and without symmetry breaking. The new findings and insights of this work include the following: (1) Symmetry-protected BICs and accident BICs at-Γ exhibiting Fano lineshapes can be simultaneously excited in Si-based metasurfaces with and without symmetry breaking. The leakage of a quasi-BIC arises from the inevitable interference of Mie resonances that limits the Q factor of the quasi-BIC. (2) The Q factors of the quasi-BICs supported in a metasurface with symmetry breaking can be manipulated by changing the period of the metasurface. The maximum Q factors achieved in the metasurface with symmetry breaking may be close to those observed in the metasurface without symmetry breaking. (3) The deviation of the period from the optimum value can be considered as an asymmetry induced in the metasurface. A deviation of the period from this optimum value will lead to an exponential reduction of the Q factor. (4) The Q factors of the quasi-BICs supported in a metasurface with symmetry breaking may increase with increasing defect size (asymmetry). As shown in this work, the Q factor of a quasi-BIC formed in a metasurface with symmetry breaking can be modified by more than 4 orders of magnitude by simply varying the period of the metasurface. Since the coupling between the constituent elements in a metasurface is sensitive to the small variation in the surrounding environment, it is expected that the exponential dependence of the Q factor on the period (or effective optical path) can be employed to realize optical sensors with high sensitivities. Our findings are important for understanding the physical origins for the quasi-BICs formed in metasurfaces and helpful for designing photonic devices with different functionalities.

METHODS

Sample Fabrication. The metasurfaces composed of Si cuboids with and without symmetry breaking were fabricated by using the combination of electron beam lithography and reactive ion etching. The detailed procedure for fabricating the metasurfaces is described in the Supporting Information (Note 16). The morphologies of the as-prepared metasurfaces were examined by SEM observations (see the Supporting Information, Note 17).

Optical Characterization. The reflection spectra of the metasurfaces were measured by using a customized free space setup. A supercontinuum source polarized in the y direction, which was employed as a broadband white light source, was focused on the targeted metasurface via a ×10 objective (Olympus) with NA = 0.30. The reflected white light was collected by using the same objective and directed to a spectrometer for spectral analysis after passing an analyzer set in the x direction. This method has been used in the characterization of the quasi-BICs supported by metasurfaces.[53]

Numerical Simulation. In this work, we studied metasurfaces with infinite sizes. Thus, we employed a periodic bound condition in the x and y directions and perfectly matched layers in the z direction to absorb the outgoing waves in the numerical simulations. In all cases, we used a plane wave propagating in the $-z$ direction to excite the metasurface. The electric and magnetic fields of the plane wave were oriented in the y and x directions, respectively. The Q factors of the quasi-BICs supported by the metasurfaces were derived by using a multiphysics software (COMSOL) from the solution of eigenfrequency. The complex eigenfrequency can be expressed as $\omega_0 + i\gamma$, where ω_0 and γ denote the real and imaginary parts of the complex eigen frequency. The Q factor was derived by $Q = \omega_0/2\gamma$. The refractive index of Si was taken from the literature,[54] while that of SiO_2 was chosen to be 1.45.

ASSOCIATED CONTENT

Supporting Information

The Supporting Information is available free of charge at https://pubs.acs.org/doi/10.1021/acsphotonics.2c01461.

Multipolar expansion analysis for the quasi-BICs in various metasurfaces; dependence of the Q factor of the quasi-BIC on the period of the metasurface; optical properties of the quasi-BICs, including Q factors, field enhancement factors, and radiation patterns; dependence of the Q factor of the quasi-BIC on the defect size; comparison of the quasi-BICs for metasurfaces with different structures; procedure for fabricating the metasurfaces; and SEM characterization of the metasurfaces (PDF)

AUTHOR INFORMATION

Corresponding Authors

Zhuojun Liu − *State Key Laboratory for Mesoscopic Physics and Frontiers Science Center for Nano-optoelectronics, School of Physics, Peking University, Beijing 100871, China*; Email: zhuojunliu@pku.edu.cn

Sheng Lan − *Guangdong Provincial Key Laboratory of Nanophotonic Functional Materials and Devices, School of Information and Optoelectronic Science and Engineering, South China Normal University, Guangzhou 510006, China*; orcid.org/0000-0002-7277-0042; Email: slan@scnu.edu.cn

Authors

Zhaotang Li − *Guangdong Provincial Key Laboratory of Nanophotonic Functional Materials and Devices, School of Information and Optoelectronic Science and Engineering,*

https://doi.org/10.1021/acsphotonics.2c01461
ACS Photonics 2023, 10, 206−216

South China Normal University, Guangzhou 510006, China; orcid.org/0000-0001-9517-553X

Lidan Zhou − *Guangdong Provincial Key Laboratory of Nanophotonic Functional Materials and Devices, School of Information and Optoelectronic Science and Engineering, South China Normal University, Guangzhou 510006, China; State Key Laboratory of Optoelectronic Materials and Technologies, School of Electronics and Information Technology, Sun Yat-sen University, Guangzhou 51006, China;* orcid.org/0000-0003-3146-9082

Mingcheng Panmai − *Guangdong Provincial Key Laboratory of Nanophotonic Functional Materials and Devices, School of Information and Optoelectronic Science and Engineering, South China Normal University, Guangzhou 510006, China*

Shulei Li − *Guangdong Provincial Key Laboratory of Nanophotonic Functional Materials and Devices, School of Information and Optoelectronic Science and Engineering, South China Normal University, Guangzhou 510006, China; School of Optoelectronic Engineering, Guangdong Polytechnic Normal University, Guangzhou 510665, China*

Jin Liu − *State Key Laboratory of Optoelectronic Materials and Technologies, School of Physics, Sun Yat-sen University, Guangzhou 510275, China;* orcid.org/0000-0001-5727-6874

Complete contact information is available at: https://pubs.acs.org/10.1021/acsphotonics.2c01461

Author Contributions

Z.L. and L.Z. contributed equally to this work. S.L. and Z.L. conceived the idea. Z.L. performed the numerical simulations, L.Z. fabricated the samples, and Z.L. carried out the optical measurements. S.L., J.L., Z.L., M.P., and S.L. analyzed the data and wrote the manuscript; S.L. and J.L. supervised the project. All the authors read and commented on the manuscript.

Funding

S.L. and Z.Liu acknowledge the financial support from the National Natural Science Foundation of China (Grant Nos 11874020, 12174123, and 12204019). Z.Liu is supported by the National Postdoctoral Program for Innovative Talents (Grant No. BX20220010) and the China Postdoctoral Science Foundation (Grant No. 2022M710233).

Notes

The authors declare no competing financial interest.

REFERENCES

(1) Koshelev, K.; Kivshar, Y. Dielectric Resonant Metaphotonics. *ACS Photonics* **2020**, *8*, 102−112.
(2) Kuznetsov, A. I.; Miroshnichenko, A. E.; Brongersma, M. L.; Kivshar, Y. S.; Luk'yanchuk, B. Optically resonant dielectric nanostructures. *Science* **2016**, *354*, aag2472.
(3) Li, A.; Singh, S.; Sievenpiper, D. Metasurfaces and Their Applications. *NANO* **2018**, *7*, 989−1011.
(4) Chen, H. T.; Taylor, A. J.; Yu, N. A Review of Metasurfaces: Physics and Applications. *Rep. Prog. Phys.* **2016**, *79*, 076401.
(5) Glybovski, S. B.; Tretyakov, S. A.; Belov, P. A.; Kivshar, Y. S.; Simovski, C. R. Metasurfaces: From Microwaves to Visible. *Phys. Rep.* **2016**, *634*, 1−72.
(6) Hsiao, H.-H.; Chu, C. H.; Tsai, D. P. Fundamentals and Applications of Metasurfaces. *Small Methods* **2017**, *1*, 1600064.
(7) Ding, F.; Pors, A.; Bozhevolnyi, S. I. Gradient Metasurfaces: A Review of Fundamentals and Applications. *Rep. Prog. Phys.* **2018**, *81*, 026401.
(8) Liu, M.; Choi, D. Y. Extreme Huygens' Metasurfaces Based on Quasi-Bound States in the Continuum. *Nano Lett.* **2018**, *18*, 8062−8069.
(9) Liang, Y.; Koshelev, K.; Zhang, F.; Lin, H.; Lin, S.; Wu, J.; Jia, B.; Kivshar, Y. Bound States in the Continuum in Anisotropic Plasmonic Metasurfaces. *Nano Lett.* **2020**, *20*, 6351−6356.
(10) Kyaw, C.; Yahiaoui, R.; Burrow, J. A.; Tran, V.; Keelen, K.; Sims, W.; Red, E. C.; Rockward, W. S.; Thomas, M. A.; Sarangan, A.; Agha, I.; Searles, T. A. Polarization-Selective Modulation of Supercavity Resonances Originating from Bound States in the Continuum. *Commun. Phys.* **2020**, *3*, 212.
(11) Chen, X.; Fan, W.; Yan, H. Toroidal Dipole Bound States in the Continuum Metasurfaces for Terahertz Nanofilm Sensing. *Opt. Express* **2020**, *28*, 17102−17112.
(12) Zhao, X.; Chen, C.; Kaj, K.; Hammock, I.; Huang, Y.; Averitt, R. D.; Zhang, X. Terahertz Investigation of Bound States in the Continuum of Metallic Metasurfaces. *Optica* **2020**, *7*, 1548−1554.
(13) Xiang, J.; Panmai, M.; Bai, S.; Ren, Y.; Li, G. C.; Li, S.; Liu, J.; Li, J.; Zeng, M.; She, J.; Xu, Y.; Lan, S. Crystalline Silicon White Light Sources Driven by Optical Resonances. *Nano Lett.* **2021**, *21*, 2397−2405.
(14) Tian, J.; Li, Q.; Belov, P. A.; Sinha, R. K.; Qian, W.; Qiu, M. High-Q All-Dielectric Metasurface: Super and Suppressed Optical Absorption. *ACS Photonics* **2020**, *7*, 1436−1443.
(15) Kodigala, A.; Lepetit, T.; Gu, Q.; Bahari, B.; Fainman, Y.; Kanté, B. Lasing Action from Photonic Bound States in Continuum. *Nature* **2017**, *541*, 196−199.
(16) Wu, M.; Ha, S. T.; Shendre, S.; Durmusoglu, E. G.; Koh, W. K.; Abujetas, D. R.; Sánchez-Gil, J. A.; Paniagua-Domínguez, R.; Demir, H. V.; Kuznetsov, A. I. Room-Temperature Lasing in Colloidal Nanoplatelets Via Mie-Resonant Bound States in the Continuum. *Nano Lett.* **2020**, *20*, 6005−6011.
(17) Bernhardt, N.; Koshelev, K.; White, S. J. U.; Meng, K. W. C.; Fröch, J. E.; Kim, S.; Tran, T. T.; Choi, D. Y.; Kivshar, Y.; Solntsev, A. S. Quasi-Bic Resonant Enhancement of Second-Harmonic Generation in WS_2 Monolayers. *Nano Lett.* **2020**, *20*, 5309−5314.
(18) Koshelev, K.; Tang, Y.; Li, K.; Choi, D.-Y.; Li, G.; Kivshar, Y. Nonlinear Metasurfaces Governed by Bound States in the Continuum. *ACS Photonics* **2019**, *6*, 1639−1644.
(19) Koshelev, K.; Bogdanov, A.; Kivshar, Y. Meta-optics and bound states in the continuum. *Sci. Bull.* **2019**, *64*, 836−842.
(20) Wang, J.; Kühne, J.; Karamanos, T.; Rockstuhl, C.; Maier, S. A.; Tittl, A. All-Dielectric Crescent Metasurface Sensor Driven by Bound States in the Continuum. *Adv. Funct. Mater.* **2021**, *31*, 2104652.
(21) Romano, S.; Zito, G.; Torino, S.; Calafiore, G.; Penzo, E.; Coppola, G.; Cabrini, S.; Rendina, I.; Mocella, V. Label-Free Sensing of Ultralow-Weight Molecules with All-Dielectric Metasurfaces Supporting Bound States in the Continuum. *Photonics Res.* **2018**, *6*, 726.
(22) Maksimov, D. N.; Gerasimov, V. S.; Romano, S.; Polyutov, S. P. Refractive Index Sensing with Optical Bound States in the Continuum. *Opt. Express* **2020**, *28*, 38907−38916.
(23) Huang, L.; Xu, L.; Rahmani, M.; Neshev, D.; Miroshnichenko, A. E. Pushing the Limit of High-Q Mode of a Single Dielectric Nanocavity. *Adv. Photonics* **2021**, *3*, 016004.
(24) Tuz, V. R.; Khardikov, V. V.; Kupriianov, A. S.; Domina, K. L.; Xu, S.; Wang, H.; Sun, H. B. High-Quality Trapped Modes in All-Dielectric Metamaterials. *Opt. Express* **2018**, *26*, 2905−2916.
(25) Forouzmand, A.; Mosallaei, H. All-Dielectric C-Shaped Nanoantennas for Light Manipulation: Tailoring Both Magnetic and Electric Resonances to the Desire. *Adv. Opt. Mater.* **2017**, *5*, 1700147.
(26) Kupriianov, A. S.; Xu, Y.; Sayanskiy, A.; Dmitriev, V.; Kivshar, Y. S.; Tuz, V. R. Metasurface Engineering through Bound States in the Continuum. *Phys. Rev. Appl.* **2019**, *12*, 014024.
(27) Wang, B.; Liu, W.; Zhao, M.; Wang, J.; Zhang, Y.; Chen, A.; Guan, F.; Liu, X.; Shi, L.; Zi, J. Generating Optical Vortex Beams by Momentum-Space Polarization Vortices Centred at Bound States in the Continuum. *Nat. Photonics* **2020**, *14*, 623−628.

(28) Huang, C.; Zhang, C.; Xiao, S.; Wang, Y.; Fan, Y.; Liu, Y.; Zhang, N.; Qu, G.; Ji, H.; Han, J.; Ge, L.; Kivshar, Y.; Song, Q. Ultrafast control of vortex microlasers. *Science* **2020**, *367*, 1018−1021.
(29) Bogdanov, A. A.; Koshelev, K. L.; Kapitanova, P. V.; Rybin, M. V.; Gladyshev, S. A.; Sadrieva, Z. F.; Samusev, K. B.; Kivshar, Y. S.; Limonov, M. F. Bound States in the Continuum and Fano Resonances in the Strong Mode Coupling Regime. *Adv. Photonics* **2019**, *1*, 016001.
(30) Carletti, L.; Koshelev, K.; De Angelis, C.; Kivshar, Y. Giant Nonlinear Response at the Nanoscale Driven by Bound States in the Continuum. *Phys. Rev. Lett.* **2018**, *121*, 033903.
(31) Rybin, M. V.; Koshelev, K. L.; Sadrieva, Z. F.; Samusev, K. B.; Bogdanov, A. A.; Limonov, M. F.; Kivshar, Y. S. High-Q Supercavity Modes in Subwavelength Dielectric Resonators. *Phys. Rev. Lett.* **2017**, *119*, 243901.
(32) Solodovchenko, N.; Samusev, K.; Bochek, D.; Limonov, M. Bound States in the Continuum in Strong-Coupling and Weak-Coupling Regimes under the Cylinder - Ring Transition. *NANO* **2021**, *10*, 4347−4355.
(33) Azzam, S. I.; Shalaev, V. M.; Boltasseva, A.; Kildishev, A. V. Formation of Bound States in the Continuum in Hybrid Plasmonic-Photonic Systems. *Phys. Rev. Lett.* **2018**, *121*, 253901.
(34) Panmai, M.; Xiang, J.; Li, S.; He, X.; Ren, Y.; Zeng, M.; She, J.; Li, J.; Lan, S. Highly Efficient Nonlinear Optical Emission from a Subwavelength Crystalline Silicon Cuboid Mediated by Supercavity Mode. *Nat. Commun.* **2022**, *13*, 2749.
(35) Koshelev, K.; Kruk, S.; Melik-Gaykazyan, E.; Choi, J.-H.; Bogdanov, A.; Park, H.-G.; Kivshar, Y. Subwavelength dielectric resonators for nonlinear nanophotonics. *Science* **2020**, *367*, 288−292.
(36) Xiang, J.; Xu, Y.; Chen, J.-D.; Lan, S. Tailoring the Spatial Localization of Bound State in the Continuum in Plasmonic-Dielectric Hybrid System. *NANO* **2020**, *9*, 133−142.
(37) Koshelev, K.; Lepeshov, S.; Liu, M.; Bogdanov, A.; Kivshar, Y. Asymmetric Metasurfaces with High-Q Resonances Governed by Bound States in the Continuum. *Phys. Rev. Lett.* **2018**, *121*, 193903.
(38) Qin, M.; Xiao, S.; Liu, W.; Ouyang, M.; Yu, T.; Wang, T.; Liao, Q. Strong Coupling between Excitons and Magnetic Dipole Quasi-Bound States in the Continuum in WS_2-TiO_2 Hybrid Metasurfaces. *Opt. Express* **2021**, *29*, 18026−18036.
(39) Ndao, A.; Hsu, L.; Cai, W.; Ha, J.; Park, J.; Contractor, R.; Lo, Y.; Kanté, B. Differentiating and Quantifying Exosome Secretion from a Single Cell Using Quasi-Bound States in the Continuum. *NANO* **2020**, *9*, 1081−1086.
(40) Ovcharenko, A. I.; Blanchard, C.; Hugonin, J.-P.; Sauvan, C. Bound States in the Continuum in Symmetric and Asymmetric Photonic Crystal Slabs. *Phys. Rev. B* **2020**, *101*, 155303.
(41) Liu, M.; Powell, D. A.; Guo, R.; Shadrivov, I. V.; Kivshar, Y. S. Polarization-Induced Chirality in Metamaterials Via Optomechanical Interaction. *Adv. Opt. Mater.* **2016**, *5*, 1600760.
(42) Koshelev, K. L.; Sychev, S. K.; Sadrieva, Z. F.; Bogdanov, A. A.; Iorsh, I. V. Strong Coupling between Excitons in Transition Metal Dichalcogenides and Optical Bound States in the Continuum. *Phys. Rev. B* **2018**, *98*, 161113.
(43) Campione, S.; Liu, S.; Basilio, L. I.; Warne, L. K.; Langston, W. L.; Luk, T. S.; Wendt, J. R.; Reno, J. L.; Keeler, G. A.; Brener, I.; Sinclair, M. B. Broken Symmetry Dielectric Resonators for High Quality Factor Fano Metasurfaces. *ACS Photonics* **2016**, *3*, 2362−2367.
(44) Zhou, C.; Qu, X.; Xiao, S.; Fan, M. Imaging through a Fano-Resonant Dielectric Metasurface Governed by Quasi-Bound States in the Continuum. *Phys. Rev. Appl.* **2020**, *14*, 044009.
(45) Liu, Z.; Xu, Y.; Lin, Y.; Xiang, J.; Feng, T.; Cao, Q.; Li, J.; Lan, S.; Liu, J. High-Q Quasibound States in the Continuum for Nonlinear Metasurfaces. *Phys. Rev. Lett.* **2019**, *123*, 253901.
(46) He, Y.; Guo, G.; Feng, T.; Xu, Y.; Miroshnichenko, A. E. Toroidal Dipole Bound States in the Continuum. *Phys. Rev. B* **2018**, *98*, 161112.
(47) Sadrieva, Z.; Frizyuk, K.; Petrov, M.; Kivshar, Y.; Bogdanov, A. Multipolar Origin of Bound States in the Continuum. *Phys. Rev. B* **2019**, *100*, 115303.
(48) Ha, S. T.; Fu, Y. H.; Emani, N. K.; Pan, Z.; Bakker, R. M.; Paniagua-Domínguez, R.; Kuznetsov, A. I. Directional Lasing in Resonant Semiconductor Nanoantenna Arrays. *Nat. Nanotechnol.* **2018**, *13*, 1042−1047.
(49) Bakker, R. M.; Yu, Y. F.; Paniagua-Domínguez, R.; Luk'yanchuk, B.; Kuznetsov, A. I. Resonant Light Guiding Along a Chain of Silicon Nanoparticles. *Nano Lett.* **2017**, *17*, 3458−3464.
(50) Wang, X.; Duan, J.; Chen, W.; Zhou, C.; Liu, T.; Xiao, S. Controlling Light Absorption of Graphene at Critical Coupling through Magnetic Dipole Quasi-Bound States in the Continuum Resonance. *Phys. Rev. B* **2020**, *102*, 155432.
(51) Vabishchevich, P. P.; Liu, S.; Sinclair, M. B.; Keeler, G. A.; Peake, G. M.; Brener, I. Enhanced Second-Harmonic Generation Using Broken Symmetry III−V Semiconductor Fano Metasurfaces. *ACS Photonics* **2018**, *5*, 1685−1690.
(52) Murai, S.; Abujetas, D. R.; Castellanos, G. W.; Sánchez-Gil, J. A.; Zhang, F.; Rivas, J. G. Bound States in the Continuum in the Visible Emerging from out-of-Plane Magnetic Dipoles. *ACS Photonics* **2020**, *7*, 2204−2210.
(53) Galli, M.; Portalupi, S. L.; Belotti, M.; Andreani, L. C.; O'Faolain, L.; Krauss, T. F. Light Scattering and Fano Resonances in High-Q Photonic Crystal Nanocavities. *Appl. Phys. Lett.* **2009**, *94*, 071101.
(54) Green, M. A. Self-Consistent Optical Parameters of Intrinsic Silicon at 300k Including Temperature Coefficients. *Sol. Energy Mater. Sol. Cells* **2008**, *92*, 1305−1310.

https://doi.org/10.1021/acsphotonics.2c01461
ACS Photonics 2023, 10, 206−216